Optical Pattern Transitions from Modulation to Transverse Instabilities in Photorefractive Crystals

Chien-Chung Jeng,[1] YuanYao Lin,[2] Ray-Ching Hong,[1] and Ray-Kuang Lee[2]
[1]*Department of Physics, National Chung-Hsing University, Taichung 402, Taiwan*
[2]*Institute of Photonics Technologies, National Tsing-Hua University, Hsinchu 300, Taiwan*
(Received 17 November 2008; published 14 April 2009)

We show by experimental measurements and theoretical analyses that there exists a pattern transition from optical modulation instability to transverse instability in nonlinear media. An input coherent beam propagating in the photorefractive crystals is observed to break up into stripe filaments at a first threshold voltage. By modeling the periodic strip filaments as cnoidal waves, we demonstrate that a second threshold voltage for forming dot filaments comes from the transverse instability, resulting in a good agreement with the experimental data.

DOI: 10.1103/PhysRevLett.102.153905 PACS numbers: 42.65.Sf, 42.70.Nq

Modulation instability (MI) is a universal signature of symmetry-breaking phenomena, which has been studied in different areas of nonlinear systems as a simple means to observe the manifestation of strongly nonlinear effects in nature [1–3]. Because of MI, a small perturbation in the amplitude or phase could cause the input waves to grow exponentially. The MI process is thus closely related to the pattern formations, including chaotic [4,5], solitary [6], and turbulence waves [7], in various area of physics [8,9]. In bulk Kerr media, MI causes a random dislocation of extended beams, which subsequently undergo a catastrophic collapse. Another instability similar to MI is the transverse instabilities (TI) of spatial optical solitons associated with the growth of transverse modulations of quasi-one-dimensional bright and dark soliton stripes. In particular, this symmetry-breaking instability turns a bright soliton stripe into an array of two-dimensional filaments [10] and bends a dark soliton stripe that evolves into pairs of optical vortices of different polarities [11]. Consequently, the transverse instability sets severe limits on the observation of spatial solitons in bulk media [12,13]. In order to demonstrate spatial-temporal solitons in higher dimensions, several different physical mechanisms have been proposed for suppressing the soliton transverse instabilities, including the effect of partial incoherence of light [14], anisotropic nonlinear response [15], and nonlocal nonlinearity in photorefractive crystals [16].

Recently, it was found that MI occurs not only with coherent beams. With a noninstantaneous response in the nonlinear medium, observations of MI with an incoherent beam are possible as long as the phase fluctuations of the beam are faster than the response time of the material [17]. Later on, a partially incoherent optical vortex was demonstrated in experiments with a self-focusing nonlinear media [18]. The spatiotemporal optical MI of coherent lights in noninstantaneous nonlinear media has been studied by one of the authors [19,20]. The modulated field evolves into periodic stripes with a small nonlinearity (biased voltage). No matter for coherent or incoherent beams, most of the studies on MI have mainly adopted an approach regarding $(1 + 1)D$ solutions. As a first step, this approximation is sufficient to explain the major effects. But as shown later for a fixed input intensity, in contrast, by increasing the biased voltage patterns in forms of dot filaments are observed under the high nonlinearity limit.

Although the orientation of MI stripes is randomly selected by the vacuum noises or material defects [17], the delayed onset of $(2 + 1)D$ filamentations via $(1 + 1)D$ stripe solutions cannot be covered. In Ref. [21], Gütlich *et al.* attribute this phenomenon to the anisotropy-induced secondary modulation instability. However, if this anisotropic effect is dominant, the MI stripes shall be orientated with a certain direction that possesses the highest MI growth rate. In this Letter we show that even in an isotropic nonlinear medium a secondary threshold voltage for stripe filaments to break up also exists. By modeling the formed MI stripe filaments as periodic cnoidal waves [22–25], on top of which we apply a TI analysis. The results show that we have a larger spatial filament vector in another axis even at a lower bias voltage with a secondary threshold voltage due to the transverse instability. Then the instabilities in the two axes possess almost the same value of spatial wave numbers at a higher bias voltage, resulting in a good agreement to experimental observations.

In the experiment, as illustrated in Fig. 1, we split a 515 nm cw Yb:YAG laser light into two beams using a polarizing beam splitter (PBS). The extraordinarily (signal) and ordinarily (background) polarized beams are collimated into a strontium-barium niobate (SBN) crystal separately to control the degree of saturation. The SBN crystal is 5 mm in length and 5 mm in thickness along the c axis, which has an effective electro-optical coefficient 350 pm/V. Consequently, the effective nonlinear refractive index due to the photoinduced space charge field is linearly proportional to an external DC field as $\Delta n = -n_0^3 r_{\mathrm{eff}} |E_{\mathrm{ext}}|/(1 + I/I_s)$, where $r_{\mathrm{eff}} \propto r_{33}$ for a SBN crys-

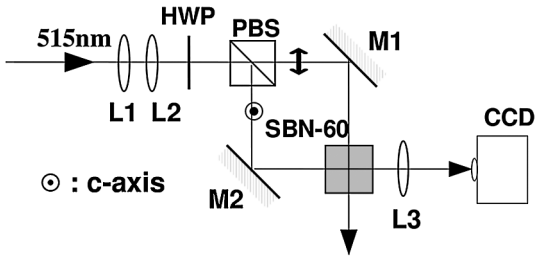

FIG. 1. Illustration of our experimental setup, where PBS is the polarization beam splitter, SBN-60 is the photorefractive crystal, HWP is a half-wave plate, L1 and L2 are two plano-convex lenses used for beam collimation, M1 and M2 are two reflecting mirrors, and L3 is an imaging lens to collect pattern images into the CCD camera.

tal [26,27]. The ratio of the input beam intensity (I) to the background beam intensity (I_s) is kept at 10 for different operations. A charge-coupled device (CCD) camera is placed after an imaging lens to capture the self-organized optical patterns at the output plane, with a 8 mm $\times$ 8 mm CCD chip size and a 330 μm $\times$ 330 μm field of view.

In Fig. 2, we demonstrate series of optical patterns recorded by the CCD camera at the output plane for input optical intensities at $I = 65$, 96, and 190 mW/cm^2, respectively. The measured patterns are formed in the following scenario. In the first row, from a plane wave input only uniform patterns with some neglected fluctuations in the image system are shown in the output plane at a very small bias voltage. Later, stripe filaments in the periodic structures are first developed with a random orientation. Subsequently, these periodic waves split and break into filaments as a result of transverse instability, to be quantitatively verified by our proposed model later. For a given crystal length, sufficient nonlinearities controlled by the applied voltage across the crystal along the c axis are required for waves to evolve into observable patterns. As shown in the second and third rows of Fig. 2, it is straightforward to expect that there should exist separated threshold voltages for stripe- and dot-filament patterns. At a higher bias voltage, in the last two rows we demonstrate the formations of optical turbulence patterns.

To explain the pattern transition from MI to TI, here we model the fields propagating in a SBN crystal by using the nonlinear Schrödinger equation (NSE) with a noninstantaneous isotropic photorefractive response [20], i.e.,

$$i\frac{\partial A}{\partial z} + \frac{1}{2}\nabla_\perp^2 A - \gamma \int_{-\infty}^{t} \frac{1}{\tau} F(|A|^2) e^{-(t-t_1)/\tau} dt_1 A = 0, \quad (1)$$

where the spatial coordinates are normalized to $1/k$ with k being the wave number of the incident field, and A is normalized to $\sqrt{I_s}$ given that I_s is the saturation intensity (as the background beam). The nonlinear strength γ is assumed to be linearly dependent on the external dc field, τ is the time constant of the system, and the nonlinear response function is given as $F = 1/(1 + |A|^2)$.

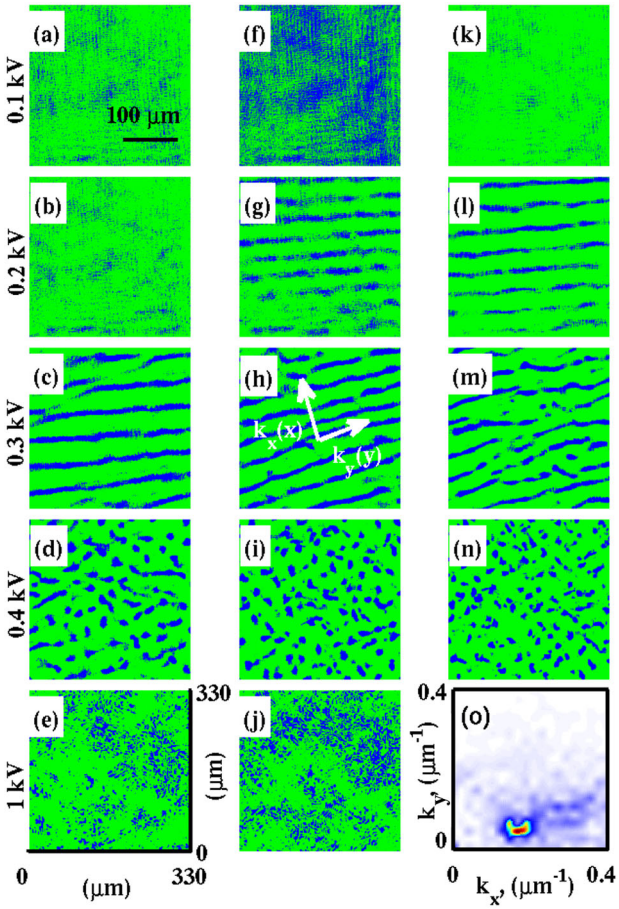

FIG. 2 (color online). The optical intensity patterns of a coherent beam at the output plane through a nonlinear crystal at different bias voltages (shown in the left column) and different input intensities: (a)–(e) 65 mW/cm^2, (f)–(j) 96 mW/cm^2, and (k)–(n) 190 mW/cm^2. The 2D Fourier transform of the experimental measurement in (h) is shown in (o), with the corresponding directions of wave vectors k_x and k_y indicated.

For MI, we use a plane wave as the input and study the corresponding instability [20]. As a consequence of MI, the plane waves turn into a chain of stripes at a spatial frequency with the maximum field growth rate along a randomly selected direction. Before symmetry-breaking instability in higher dimensions deteriorates the optical patterns severely, the stationary periodic waves can be formed in nonlinear materials known as *cnoidal waves*, which was first introduced by Kortweg and de Vries in their works of *cnoidal wave theory* [28]. Recently, the stability of multicomponent photorefractive cnoidal waves were formulated with a drift nonlinear response [29]. As for the strip filaments formed by MI in the periodic structures, for TI, we adopt this concept by assuming a preformed cnoidal wave on top of fully developed MI patterns as solutions to the NSE, i.e., $A_0 = \phi(x)e^{-i\beta z}$, where $\phi(x + L) = \phi(x)$ and L is the spatial period. The stationary cnoidal wave solution A_0 adopted here is of *cn-type* for that with a saturable nonlinearity only cnoidal waves of

cn-type are stable when its power flow exceed a certain threshold [30]. Then again we calculate the instability spectrum of cnoidal waves in the NSE by using the standard linear stability analysis, i.e., $A = A_0 + \Delta A$, where

$$\Delta A = [(v + iw)e^{ik_y y + i\lambda z + i\Omega t} + (v^* + iw^*)e^{-ik_y y - i\lambda^* z - i\Omega t}]e^{-i\beta z}$$

with the transverse wave number k_y and the frequency of the perturbed field Ω. Then a set of linear coupled equations can be obtained by linearizing the NSE in Eq. (1), i.e.,

$$\lambda\tilde{w} = [L_1 - \tfrac{1}{2}k_y^2]v, \quad \text{and} \quad \lambda v = [L_0 - \tfrac{1}{2}k_y^2]\tilde{w}, \qquad (2)$$

where $\tilde{w} = iw$, $L_0 = \beta + \frac{1}{2}\nabla_\perp^2 + F_0$, $L_1 = L_0 + \frac{2F_0'A_0^2}{i\Omega+1}$, $F_0 = F(|A_0|^2)$, and $F_0' = \frac{dF}{d|A|^2}_{A=A_0}$. By expansions at the neutral modes [31,32],

$$\tilde{w} = \tilde{w}_0 + \lambda\tilde{w}_1 + \mathbf{O}(\lambda^2), \quad \text{and} \quad v = v_0 + \lambda v_1 + \mathbf{O}(\lambda^2), \qquad (3)$$

in which $\tilde{w}_0 = A_0$ and $v_0 = 0$. We readily obtain $v_1 = (L_0 + \frac{2F_0'A_0^2}{i\Omega+1})^{-1}\tilde{w}_0$ after substituting Eq. (3) into the linearized equations in Eq. (2) to the first order of λ. The dependence of the TI growth rate of cn-type cnoidal waves to the transverse wave number k_y can be derived asymptotically in the following,

$$\lambda^2 = -\frac{1}{2}\frac{(A_0, A_0)}{(A_0, L_1^{-1}A_0)}k_y^2 - \frac{1}{4}k_y^4, \qquad (4)$$

where the operation $(w, v) \equiv \int_{-\infty}^{\infty} w^* v dx$, and we have a simple formula in the second term as the case derived for the cubic nonlinearity [32]. The imaginary part of λ contributes to the field growth rate which we denoted as h_y hereafter.

Figure 3(a) shows the spatial wave number k_x with the maximum field growth rate h_x of the MI for plane waves in a photorefractive material at $I/I_s = 10$ and $\Omega\tau = 0$ for different nonlinearities. It is seen that both the spatial wave number and field growth rate increase with the nonlinearity. Despite the fact that the growth rate decreases when $\Omega\tau$ increases in the noninstantaneous medium, the spatial wave number k_x with a maximum growth rate is independent of $\Omega\tau$ [20]. Then a cn-type cnoidal wave, shown in the inset of Fig. 3(c), is developed at these spatial frequencies associated with the maximum field growth rate, i.e., $L = 1/k_x^{\max}$, and the corresponding transverse instability is demonstrated in Fig. 3(b) for $\Omega\tau = 0$. It is clearly seen that the maximum growth rate for the cnoidal wave TI is much smaller than that of the plane wave MI at the same input intensity and nonlinearity. However, the value of spatial wave number k_y approaches k_x even we use an isotropic model here. This indicates that fully evolved patterns are isotropically self-organized and the density of dot filaments increases at a higher nonlinearity, as supported by experimental results in the fourth row of Fig. 2 and in Fig. 3 by the spatial and momentum distributions, respectively. In addition, for a finite crystal length, there shall exist two threshold nonlinearities for observed stripe- and dot-filament patterns to develop, due to different maximum growth rates in the two axes. In Fig. 3(c), we show the TI spectra of cnoidal waves at $\gamma = 1$ and $I/I_s = 10$ for different frequency-time-constant products, $\Omega\tau$. Very similar to the plane wave MI [20], the growth rate of cnoidal wave TI decreases when $\Omega\tau$ increases for the noninstantaneous response of the photorefractive crystals. And again the spatial wave number with a maximum growth rate is independent of $\Omega\tau$ with the asymptotic approximation as,

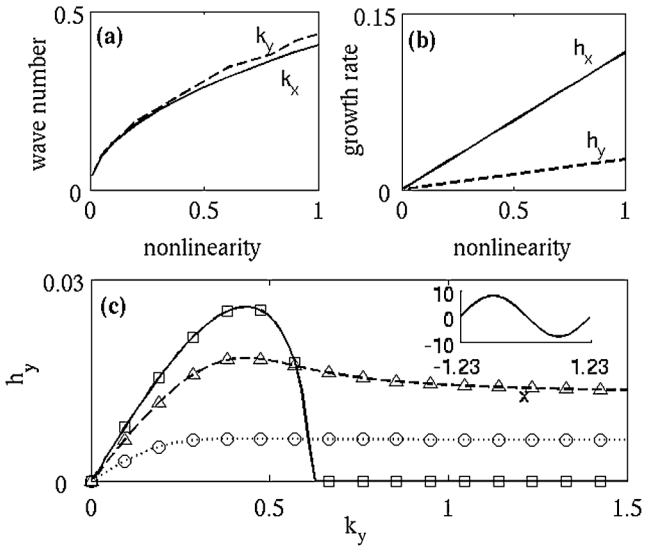

FIG. 3. (a) The spatial wave numbers with the maximum growth rate of plane wave MI (k_x, solid line) and cnoidal wave TI (k_y, dashed line), and (b) the corresponding growth rates for MI (h_x, solid line) and TI (h_y, dashed line) versus different nonlinearities in isotropic photorefractive crystals at $\Omega\tau = 0$ and $\gamma = 1$. (c) Direct numerical simulations of transverse instability spectra for cn-type cnoidal waves with a noninstantaneous response function, i.e., the frequency-time-constant products $\Omega\tau$ are 0 (solid), 1 (dashed), and 4 (dotted), respectively. The analytical results based on the asymptotic expansion method are marked by squares, triangles, and circles accordingly. The inset in (c) denotes the periodic stationary solution A_0.

$$k_y^{\max} = \sqrt{-\tfrac{1}{2}(A_0, A_0)/(A_0, (L_0 + 2F_0'A_0^2)^{-1}A_0)}. \qquad (5)$$

To manifest the insights of the transition from MI to TI, in Fig. 4, we analyze the two-dimensional spatial spectrum of measured patterns by using a 2D Fourier transformation of experimental data obtained in Fig. 2. The threshold nonlinearity (voltage) in the k_x can be read from the fitting curves in Fig. 4 as 0.19, 0.117, and 0.067 kV for $I = 65$, 96 and 190 mW/cm^2, respectively. While in the k_y, we have 0.23, 0.17, and 0.108 kV as a second threshold voltage, separately. In the spectrum, it is found that at a higher

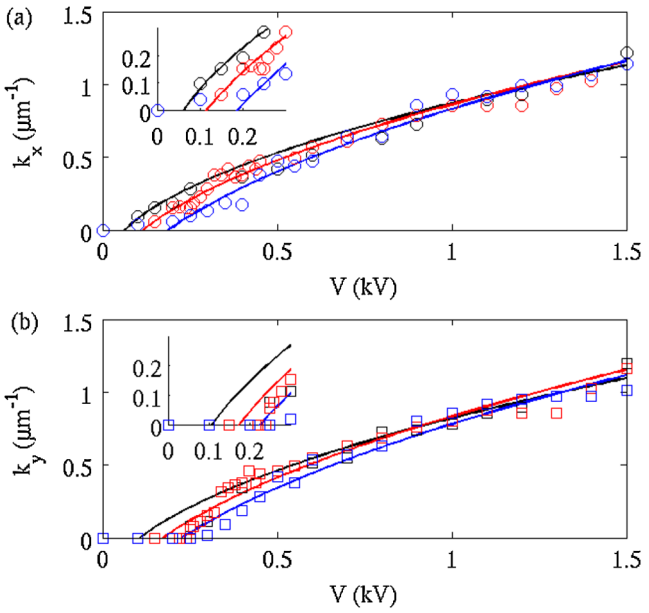

FIG. 4 (color online). Spectra of transverse patterns obtained from experimental data for (a) k_x and (b) k_y. Circles and squares markers accompanied by the fitted curves in black, red, and blue refer to optical intensities $I = 190$, 96, and 65 mW/cm^2, respectively.

nonlinearity the spatial wave numbers k_x and k_y almost have the same value where uniform dot-filament patterns are observed. In contrast, while the nonlinearity is low, the two wave numbers differ with different threshold voltages. Concerning different optical intensities, the spatial wave vectors experience very little variations in their tendencies and magnitudes because of a notable fact that they all share the same (input)/(background) ratio, $I/I_s = 10$, and represent the same normalized wave functions in the photorefractive model used in Eq. (1). Nevertheless, the threshold nonlinearities drop at a strong optical intensity due to the fact that the system time constant, τ, also drops accordingly [21]. In accordance with a lower growth rate in TI and associated with a broaden TI spectrum, it is hard to build up transverse patterns in such a case.

It is well known that it is almost impossible to see the evolutions of an input plane wave evolving in forms of stripe filaments to dot filaments just by a perturbative analysis or a direct numerical simulation. On the contrary, the approach we used here seems unnatural at a first glance for assuming a periodic wave as the MI pattern. As long as periodic strip filaments form, our proposed cnoidal wave model to explain the pattern transitions from MI to TI works. It turns out that the preformed periodic waves on top of MI patterns give us a satisfied comparisons with experiments not only qualitatively but also quantitatively. And the results we showed theoretically and experimentally here can also be useful for studying spatial-temporal pattern formations in higher dimensions for optical bullets [33,34], fluid dynamics [35], and plasma physics [36].

In summary, the formation of optical dot-filament patterns in photorefractive crystals is explained by our two stage MI to TI model in $(2 + 1)D$. We show that the spatial wave number of the transverse pattern is independent of the optical intensity and there exist two threshold nonlinearities (voltages) that clearly distinguish the MI and TI formations, respectively. With direct numerical simulations and asymptotic analyses on the modeling of plane wave MI and cnoidal wave TI, the reported pattern transitions are supported by experimental demonstrations.

[1] V. I. Bespalov and V. I. Talanov, JETP Lett. **3**, 307 (1966).
[2] V. I. Karpman, JETP Lett. **6**, 277 (1967).
[3] G. P. Agrawal, *Nonlinear Fiber Optics* (Academic Press, San Diego, 1995), 2nd ed..
[4] F. T. Arecchi *et al.*, Phys. Rev. Lett. **65**, 2531 (1990).
[5] P. L. Ramazza *et al.*, Phys. Rev. A **53**, 400 (1996).
[6] Yu. S. Kivshar and D. E. Pelinovsky, Phys. Rep. **331**, 117 (2000), and references therein.
[7] D. A. Roberts *et al.*, Phys. Rev. Lett. **67**, 3741 (1991).
[8] M. C. Cross and P. Hohenberg, Rev. Mod. Phys. **65**, 851 (1993).
[9] S. Residori, Phys. Rep. **416**, 201 (2005).
[10] A. V. Mamaev *et al.*, Phys. Rev. A **54**, 870 (1996).
[11] V. Tikhonenko *et al.*, Opt. Lett. **21**, 1129 (1996).
[12] V. E. Zakharov and A. M. Rubenchik, JETP **38**, 494 (1974).
[13] Yu. S. Kivshar and G. P. Agrawal, *Optical Solitons: from Fibers to Photonic Crystals* (Academic Press, San Diego, 2003).
[14] J. P. Torres *et al.*, Phys. Rev. E **65**, 015601(R) (2001).
[15] K. Motzek *et al.*, Opt. Lett. **29**, 280 (2004).
[16] Y. Y. Lin *et al.*, J. Opt. Soc. Am. B **25**, 576 (2008).
[17] D. Kip *et al.*, Science **290**, 495 (2000).
[18] C.-C. Jeng *et al.*, Phys. Rev. Lett. **92**, 043904 (2004).
[19] W.-H. Chu *et al.*, Opt. Lett. **30**, 1846 (2005).
[20] M. F. Shih *et al.*, Phys. Rev. Lett. **88**, 133902 (2002).
[21] B. Gütlich *et al.*, Opt. Commun. **255**, 57 (2005).
[22] V. Vysloukh *et al.*, Quantum Electron. **28**, 1034 (1998).
[23] V. Vysloukh *et al.*, Quantum Electron. **29**, 613 (1999).
[24] N. M. Litchinitser *et al.*, Phys. Rev. E **60**, 2377 (1999).
[25] V. A. Aleshkevich *et al.*, Quantum Electron. **31**, 257 (2001).
[26] C. Denz, M. Schwab, and C. Weilnau, *Transverse-Pattern Formation in Photorefractive Optics* (Springer-Verlag, Berlin Heidelberg, 2003).
[27] P. Gunter and J. P. Huignard, *Photorefractive Materials and their Applications* (Springer Science, Berlin, 2006).
[28] J. P. Byod, Physica (Amsterdam) **21D**, 227 (1986).
[29] V. M. Petnikova *et al.*, Phys. Rev. E **60**, 1009 (1999).
[30] Y. V. Kartashov *et al.*, J. Opt. B **6**, s279 (2004).
[31] G. Schmidt, Phys. Rev. Lett. **34**, 724 (1975).
[32] S. J. Han, Phys. Rev. A **20**, 2568 (1979).
[33] B. A. Malomed *et al.*, J. Opt. B **7**, R53 (2005).
[34] Y. Silberberg, Opt. Lett. **15**, 1282 (1990).
[35] T. B. Benjamin and J. E. Feir, J. Fluid Mech. **27**, 417 (1967).
[36] T. Taniuti and H. Washimi, Phys. Rev. Lett. **21**, 209 (1968).